Submitted to the IEEE Transactions on Control Systems Technology

Observer-Based Adaptive Control of a Variable Reluctance Motor: Experimental Results

Ruth Milman **Scott A. Bortoff** *

Department of Electrical and Computer Engineering
University of Toronto, Toronto, Ontario M5S 3G4 Canada
milman@control.toronto.edu bortoff@control.toronto.edu

July 31, 1997

Abstract

This paper presents experimental results for two adaptive nonlinear controllers applied to a variable reluctance motor (VRM). The first controller requires both rotor position and velocity (full state) feedback, while the latter is an observer-based backstepping-type output feedback controller, requiring only rotor position measurement. Velocity for the full-state controller is estimated using a high-gain "differentiating filter." The experimental comparison shows that the observer-based controller provides a better transient response, a smaller steady-state tracking error when gains for both controllers are comparable.

Adaptive nonlinear control theory has developed rapidly in the last five years, and the state-of-the-art is now readily available in textbook form [1]. Experimental verification of these theoretical advances has occurred in parallel. Examples include induction motor control [2], variable reluctance motor (VRM) control [3, 4, 5, 6, 7, 8, 9], and active automobile suspension [10]. Indeed, the popularity of nonlinear benchmark problems, e.g. [11], and associated conference special sessions testifies to the strong interest in such experimental verification.

*This research supported by the Natural Sciences and Engineering Research Council of Canada (NSERC) under grant OGP0138423. Please direct all correspondence to the second author.

In this paper, we present experimental results for two different adaptive nonlinear controllers applied to a VRM test bed. The control problem is trajectory tracking: Given a reference rotor angular trajectory $y_r(t)$ (and $\dot{y}_r(t)$, $\ddot{y}_r(t)$), synthesize a feedback controller to cause $y(t) \to y_r(t)$. The first result is an adaptive feedback linearization, originally presented in [9], which requires full-state measurement. However, our VRM lacks a tachometer; only the rotor position is actually measured. Rotor *velocity* is "measured" by numerically differentiating the position signal, a common approach in electro-mechanical systems. We show that this practice results in parameter drift, large tracking error, and even instability. Our second result is an observer-based backstepping-type adaptive controller which produces estimates of rotor velocity. We show that the latter controller provides improved transient and steady-state performance.

Section 1 presents our VRM model, followed by derivations of the controllers. The adaptive feedback linearizing result appears in greater detail in [9], so our development here is terse. Our experimental results are detailed in Section 2, and conclusions are drawn in Section 3.

1 Controller Development

Adopting the notation of [1, 12], we model the VRM as

$$\begin{aligned} \dot{x}_1 &= x_2 && (1) \\ \dot{x}_2 &= \sigma_l(y)\,\theta_l + \left(\sum_{i=1}^{L} \sigma_i(y) \boldsymbol{B}^T(u_i) \right) \boldsymbol{\theta}_u && (2) \\ y &= x_1, && (3) \end{aligned}$$

where x_1 and x_2 are the rotor position and velocity, respectively, and u_i, $1 \leq i \leq L$ is the i^{th} phase current, assumed to be a control input. (This is justified in [13], and by our use of current amplifiers.) The nonlinear term $\sigma_i(y)\boldsymbol{B}^T(u_i)\boldsymbol{\theta}_u$ models the acceleration generated by the i^{th} stator phase, and is proportional to torque because the rotor inertia is assumed to be constant. Similarly, $\sigma_l(y)\theta_l$ represents the load acceleration. Despite the misnomer, we refer to $\sigma_i(y)\boldsymbol{B}^T(u_i)\boldsymbol{\theta}_u$ as the "electric torque," and $\sigma_l(y)\theta_l$ as the "load torque."

The electric torque is a product of three terms: the first term in a Fourier series in y,

$$\sigma_i(y) = \sin(Py - \frac{2\pi i}{L}),$$

which captures the periodic relationship between electric torque and rotor position; a vector $\boldsymbol{\theta}_u$ of unknown coefficients; and a vector of quadratic B-splines,

$$\boldsymbol{B}(u_i) = [b_1(u_i)\ b_2(u_i)\ \cdots\ b_M(u_i)]^T,$$

which models the nonlinear relationship between electric torque and current. Here, $b_j(u_i)$ is the j^{th} quadratic B-spline basis function,

$$\begin{aligned} b_j(u_i) &= n\left(\frac{u_i - (j-1)\delta}{3\delta}\right), \\ n(s) &= \begin{cases} 0 & \text{for } s < 0 \text{ or } s > 1 \\ 9s^2/2 & \text{for } s \in [0, 1/3] \\ (-18s^2 + 18s - 3)/2 & \text{for } s \in (1/3, 2/3] \\ (3 - 3s)^2/2 & \text{for } s \in (2/3, 1], \end{cases} \end{aligned}$$

M is the number of spline intervals, δ is the interval size, and P is the number of VRM motor poles. Higher-order Fourier harmonics are easily incorporated — in [9], we use 3 — but the additional notation obscures our development. We refer the reader to [3, 6, 9] and related results for more comprehensive discussion of VRM modeling.

The load torque is the product of a known function $\sigma_l(y)$, and the unknown parameter θ_l. Note that any velocity-dependent terms are neglected. For our experiments, $\sigma_l(y) = -\sin(y)$ represents a gravitational load (a pendulum), and viscous damping is very small.

1.1 Full-State Adaptive Control

This development summarizes the results in [9]. Denoting the parameter estimates as $\widehat{\theta}_l$ and $\widehat{\boldsymbol{\theta}}_u$, and parameter errors as $\widetilde{\theta}_l = \theta_l - \widehat{\theta}_l$ and $\widetilde{\boldsymbol{\theta}}_u = \boldsymbol{\theta}_u - \widehat{\boldsymbol{\theta}}_u$, (2) can be rewritten

$$\dot{x}_2 = \sigma_l(y)\,\widehat{\theta}_l + \left(\sum_{i=1}^{L}\sigma_i(y)\boldsymbol{B}^T(u_i)\right)\widehat{\boldsymbol{\theta}}_u + \sigma_l(y)\,\widetilde{\theta}_l + \left(\sum_{i=1}^{L}\sigma_i(y)\boldsymbol{B}^T(u_i)\right)\widetilde{\boldsymbol{\theta}}_u. \quad (4)$$

Define the "outer-loop" signal

$$v = -c_{f1}(y_r - x_1) - c_{f2}(\dot{y}_r - x_2) + \ddot{y}_r, \tag{5}$$

where $s^2 + c_{f2}s + c_{f1}$ is Hurwitz, and equate the first two terms on the right-hand side of (4) with v:

$$\sigma_l(y)\,\widehat{\theta}_l + \left(\sum_{i=1}^{L} \sigma_i(y)\boldsymbol{B}^T(u_i)\right)\,\widehat{\boldsymbol{\theta}}_u = v. \tag{6}$$

This is solved for u_i, $1 \le i \le L$ using so-called *torque-sharing functions* (which define the electronic commutation), and by inverting one or more of the B-spline functions. In practice, this inversion involves computing the real roots of a quadratic, and is beyond our scope. See [6, 9] and related results for details.

Substituting (5) into (4) and rewriting (4) in the error coordinates $e_1 = x_1 - y_r$ and $e_2 = x_2 - \dot{y}_r$ gives

$$\begin{bmatrix} \dot{e}_1 \\ \dot{e}_2 \end{bmatrix} = \underbrace{\begin{bmatrix} 0 & 1 \\ -c_{f1} & -c_{f2} \end{bmatrix}}_{\boldsymbol{A}_f} \underbrace{\begin{bmatrix} e_1 \\ e_2 \end{bmatrix}}_{\boldsymbol{e}} + \underbrace{\begin{bmatrix} 0 \\ 1 \end{bmatrix}}_{\boldsymbol{B}_f} \underbrace{\left(\sigma_l(y)\,\widetilde{\theta}_l + \left(\sum_{i=1}^{L} \sigma_i(y)\boldsymbol{B}^T(u_i)\right)\,\widetilde{\boldsymbol{\theta}}_u\right)}_{\widetilde{\boldsymbol{\theta}}^T\boldsymbol{\omega}}, \tag{7}$$

where the subscript f, denoting "full-state," is introduced to discriminate between terms for the full-state feedback controller, and the observer-based controller derived in the next section. Defining a positive definite 2×2 matrix $\boldsymbol{Q}_f$, we solve $\boldsymbol{A}_f^T\boldsymbol{P}_f + \boldsymbol{P}_f\boldsymbol{A}_f + \boldsymbol{Q}_f = 0$ for $\boldsymbol{P}_f$, and define the Liapunov candidate $V = \boldsymbol{e}^T\boldsymbol{P}_f\boldsymbol{e} + \frac{1}{g_u}\widetilde{\boldsymbol{\theta}}_u^T\widetilde{\boldsymbol{\theta}}_u + \frac{1}{g_l}\widetilde{\theta}_l^T\widetilde{\theta}_l$. Differentiating V by time and defining

$$\begin{aligned} \dot{\widehat{\theta}}_l &= g_l\,\epsilon\,\sigma_l(y) & (8) \\ \dot{\widehat{\boldsymbol{\theta}}}_u &= g_u\,\epsilon\,\left(\sum_{i=1}^{L} \sigma_i(y)\boldsymbol{B}^T(u_i)\right) & (9) \end{aligned}$$

gives $\dot{V} = -\boldsymbol{e}^T\boldsymbol{Q}_f\boldsymbol{e}$, where $\epsilon = \boldsymbol{B}^T\boldsymbol{P}_f\boldsymbol{e}$.

In practice, x_2 is not directly measured. Instead, $y = x_1$ is measured, and x_2 is estimated with a numerical time derivative of y, e.g.

$$\widehat{x}_2(t) = \frac{\omega_0^2 s}{s^2 + 1.4\omega_0 s + \omega_0^2}\,[y(t)], \tag{10}$$

where $\widehat{x}_2$ denotes an estimate of x_2, and the cut-off frequency ω_0 is large relative to the system's dynamics. When $\widehat{x}_2$ replaces x_2 in (8)-(9), the map between $\widetilde{\boldsymbol{\theta}}^T \boldsymbol{\omega}$ and ϵ loses its strictly-positive-real property, which can result in parameter drift and loss of stability. Moreover, the bandwidth of the closed-loop system is large, because the feedback control is static. This can excite unmodeled dynamics, resulting in large steady-state errors and parameter drift. Our experimental results presented in Section 2 exhibit all of these effects.

1.2 Observer-Based Adaptive Control

The development in this section is a straight-forward application of the results in [1], Chapter 8. In order to construct an adaptive observer-backstepping controller for (1), we first need to design an observer with exponentially stable error dynamics. Consider the signal

$$\widehat{\boldsymbol{x}}(t) \quad = \quad \boldsymbol{\xi}(t) + \boldsymbol{\lambda}(t)\,\theta_l + \boldsymbol{\nu}(t)\,\boldsymbol{\theta}_u, \tag{11}$$

where $\boldsymbol{\xi} \in \mathcal{R}^2$ denotes the known part of the observer, $\boldsymbol{\lambda} \in \mathcal{R}^2$ denotes the part of the observer dependent on the loading parameter θ_l and $\boldsymbol{\nu} \in \mathcal{R}^{2\times M}$ denotes the part of the observer dependent on the spline coefficients $\boldsymbol{\theta}_u$. In (11), parameters θ_l and $\boldsymbol{\theta}_u$ are the true unknown parameters, so $\widehat{\boldsymbol{x}}$ can not be calculated. Rather we implement individual filter banks for $\boldsymbol{\xi}$, $\boldsymbol{\lambda}$ and $\boldsymbol{\nu}$, as follows:

$$\dot{\boldsymbol{\xi}} \quad = \quad \boldsymbol{A}\boldsymbol{\xi} + \boldsymbol{K}(y - \xi_1) \tag{12}$$

$$\dot{\boldsymbol{\lambda}} \quad = \quad \boldsymbol{A}\boldsymbol{\lambda} - \boldsymbol{K}\lambda_1 + \begin{bmatrix} 0 \\ \sigma_l \end{bmatrix} \tag{13}$$

$$\dot{\boldsymbol{\nu}} \quad = \quad \boldsymbol{A}\boldsymbol{\nu} - \boldsymbol{K}\nu_1 + \begin{bmatrix} 0 \\ \sum_{i=1}^{L} \sigma_i(y)\boldsymbol{B}^T(u_i) \end{bmatrix}, \tag{14}$$

where $\boldsymbol{A} = \begin{bmatrix} 0 & 1 \\ 0 & 0 \end{bmatrix}$ and $\boldsymbol{K} = \begin{bmatrix} k_1 \\ k_2 \end{bmatrix}$.

Defining the error $\boldsymbol{\varepsilon} = \boldsymbol{x} - \widehat{\boldsymbol{x}}$, the observer error dynamics are given by

$$\dot{\boldsymbol{\varepsilon}} \quad = \quad \dot{\boldsymbol{x}} - \dot{\widehat{\boldsymbol{x}}} \tag{15}$$

$$
\begin{aligned}
&= \dot{\boldsymbol{x}} - \Big(A(\boldsymbol{\xi} + \boldsymbol{\lambda}\theta_l + \boldsymbol{\nu}\boldsymbol{\theta}_u) + \boldsymbol{K}\big(y - (\xi_1 + \lambda_1\theta_l + \nu_1\boldsymbol{\theta}_u)\big) \\
&\quad + \begin{bmatrix} 0 \\ \sigma_l(y) \end{bmatrix} \theta_l + \begin{bmatrix} 0 \\ \sum_{i=1}^{L} \sigma_i(y)\boldsymbol{B}^T(u_i) \end{bmatrix} \boldsymbol{\theta}_u \Big) \qquad (16) \\
&= \boldsymbol{A\varepsilon} + \boldsymbol{K}\varepsilon_1 \qquad (17)
\end{aligned}
$$

$$
\dot{\boldsymbol{\varepsilon}} = \boldsymbol{A}_0\boldsymbol{\varepsilon} \qquad (18)
$$

where $\boldsymbol{A}_0 = \begin{bmatrix} -k_1 & 1 \\ -k_2 & 0 \end{bmatrix}$, and $s^2 + k_1 s + k_2$ is Hurwitz.

With the exponentially stable observer error system in place, we can design our adaptive backstepping controller. The first step is the definition of the coordinate transformation

$$
z_1 = y - y_r \qquad (19)
$$

$$
z_2 = \nu_2\widehat{\boldsymbol{\theta}}_u - \dot{y}_r - \alpha_1 \qquad (20)
$$

where α_1 is a virtual control as yet undefined. The intermediate Liapunov function is

$$
V_1 = \frac{1}{2}z_1^2 + \frac{1}{2g_l}\widetilde{\theta}_l^2 + \frac{1}{2g_u}\widetilde{\boldsymbol{\theta}}_u^T\widetilde{\boldsymbol{\theta}}_u + \frac{1}{d_1}\boldsymbol{\varepsilon}^T\boldsymbol{P}_0\boldsymbol{\varepsilon} \qquad (21)
$$

where $\boldsymbol{P}_0 \in \mathcal{R}^{2\times 2}$, $\boldsymbol{P}_0 > 0$ is chosen such that $\boldsymbol{P}_0 = \boldsymbol{P}_0^T$ and $\boldsymbol{P}_0\boldsymbol{A}_0 + \boldsymbol{A}_0^T\boldsymbol{P}_0 = -\boldsymbol{I}$. Differentiating V_1 by time,

$$
\begin{aligned}
\dot{V}_1 &= z_1\dot{z}_1 + \widetilde{\theta}_l(-\frac{1}{g_l}\dot{\widehat{\theta}}_l) + \widetilde{\boldsymbol{\theta}}_u^T(-\frac{1}{g_u}\dot{\widehat{\boldsymbol{\theta}}}_u) - \frac{1}{d_1}\boldsymbol{\varepsilon}^T\boldsymbol{\varepsilon} \\
&= z_1(\dot{y} - \dot{y}_r) + \widetilde{\theta}_l(-\frac{1}{g_l}\dot{\widehat{\theta}}_l) + \widetilde{\boldsymbol{\theta}}_u^T(-\frac{1}{g_u}\dot{\widehat{\boldsymbol{\theta}}}_u) - \frac{1}{d_1}\boldsymbol{\varepsilon}^T\boldsymbol{\varepsilon}, \qquad (22)
\end{aligned}
$$

and substituting $\dot{y} = \dot{x}_1 = x_2 = \widehat{x}_2 + \varepsilon_2 = \xi_2 + \lambda_2\theta_l + \nu_2\boldsymbol{\theta}_u + \varepsilon_2$ gives

$$
\begin{aligned}
\dot{V}_1 &= z_1(\xi_2 + \lambda_2\theta_l + \nu_2\boldsymbol{\theta}_u + \varepsilon_2 - \dot{y}_r) + \widetilde{\theta}_l(-\frac{1}{g_l}\dot{\widehat{\theta}}_l) + \widetilde{\boldsymbol{\theta}}_u^T(-\frac{1}{g_u}\dot{\widehat{\boldsymbol{\theta}}}_u) - \frac{1}{d_1}\boldsymbol{\varepsilon}^T\boldsymbol{\varepsilon} \\
&= z_1(\xi_2 + \lambda_2\widetilde{\theta}_l + \lambda_2\widehat{\theta}_l + \nu_2\widetilde{\boldsymbol{\theta}}_u + \nu_2\widehat{\boldsymbol{\theta}}_u + \varepsilon_2 - \dot{y}_r) - \frac{1}{d_1}\boldsymbol{\varepsilon}^T\boldsymbol{\varepsilon} \\
&\quad + \widetilde{\theta}_l(-\frac{1}{g_l}\dot{\widehat{\theta}}_l) + \widetilde{\boldsymbol{\theta}}_u^T(-\frac{1}{g_u}\dot{\widehat{\boldsymbol{\theta}}}_u) \\
&= z_1(\nu_2\widehat{\boldsymbol{\theta}}_u - \dot{y}_r - \alpha_1 + \alpha_1 + \xi_2 + \lambda_2\widehat{\theta}_l) + z_1\varepsilon_2 - \frac{1}{d_1}\boldsymbol{\varepsilon}^T\boldsymbol{\varepsilon} \\
&\quad + \widetilde{\theta}_l(z_1\lambda_2 - \frac{1}{g_l}\dot{\widehat{\theta}}_l) + \widetilde{\boldsymbol{\theta}}_u^T(z_1\nu_2^T - \frac{1}{g_u}\dot{\widehat{\boldsymbol{\theta}}}_u)
\end{aligned}
$$

$$\begin{aligned} &= z_1(z_2+\alpha_1+\xi_2+\lambda_2\widehat{\theta}_l)+z_1\varepsilon_2-\frac{1}{d_1}\boldsymbol{\varepsilon}^T\boldsymbol{\varepsilon} \\ &\quad +\widetilde{\theta}_l(z_1\lambda_2-\frac{1}{g_l}\dot{\widehat{\theta}}_l)+\widetilde{\boldsymbol{\theta}}_u^T(z_1\nu_2^T-\frac{1}{g_u}\dot{\widehat{\boldsymbol{\theta}}}_u). \end{aligned} \tag{23}$$

The first virtual control is defined as $\alpha_1 = -c_1 z_1 - d_1 z_1 - (\xi_2 + \lambda_2\widehat{\theta}_l)$, which gives

$$\begin{aligned} \dot{V}_1 &= -c_1 z_1^2 + z_2 z_1 - d_1 z_1^2 + z_1\varepsilon_2 - \frac{1}{d_1}\boldsymbol{\varepsilon}^T\boldsymbol{\varepsilon} \\ &\quad +\widetilde{\theta}_l(z_1\lambda_2-\frac{1}{g_l}\dot{\widehat{\theta}}_l)+\widetilde{\boldsymbol{\theta}}_u^T(z_1\nu_2^T-\frac{1}{g_u}\dot{\widehat{\boldsymbol{\theta}}}_u) \\ &= -c_1 z_1^2 + z_2 z_1 - d_1(z_1^2 - z_1\varepsilon_2 + \frac{1}{4d_1^2}\varepsilon_2^2) + \frac{1}{4d_1}\varepsilon_2^2 - \frac{1}{d_1}\boldsymbol{\varepsilon}^T\boldsymbol{\varepsilon} \\ &\quad +\widetilde{\theta}_l(z_1\lambda_2-\frac{1}{g_l}\dot{\widehat{\theta}}_l)+\widetilde{\boldsymbol{\theta}}_u^T(z_1\nu_2^T-\frac{1}{g_u}\dot{\widehat{\boldsymbol{\theta}}}_u) \\ &= -c_1 z_1^2 + z_2 z_1 - d_1(z_1 - \frac{1}{2d_1}\varepsilon_2)^2 + \frac{1}{4d_1}\varepsilon_2^2 - \frac{1}{d_1}\varepsilon_1^2 - \frac{1}{d_1}\varepsilon_2^2 \\ &\quad +\widetilde{\theta}_l(z_1\lambda_2-\frac{1}{g_l}\dot{\widehat{\theta}}_l)+\widetilde{\boldsymbol{\theta}}_u^T(z_1\nu_2^T-\frac{1}{g_u}\dot{\widehat{\boldsymbol{\theta}}}_u) \\ &\le -c_1 z_1^2 + z_2 z_1 - \frac{3}{4d_1}\boldsymbol{\varepsilon}^T\boldsymbol{\varepsilon} + \widetilde{\theta}_l(z_1\lambda_2-\frac{1}{g_l}\dot{\widehat{\theta}}_l)+\widetilde{\boldsymbol{\theta}}_u^T(z_1\nu_2^T-\frac{1}{g_u}\dot{\widehat{\boldsymbol{\theta}}}_u). \end{aligned} \tag{24}$$

In the second stage of the design, V_1 is augmented to include z_2 and an additional damping term,

$$V_2 = V_1 + \frac{1}{2}z_2^2 + \frac{1}{d_2}\boldsymbol{\varepsilon}^T\boldsymbol{P}_0\boldsymbol{\varepsilon}. \tag{25}$$

Differentiating V_2 by time gives

$$\begin{aligned} \dot{V}_2 &\le -c_1 z_1^2 - \frac{3}{4d_1}\boldsymbol{\varepsilon}^T\boldsymbol{\varepsilon} + z_2(z_1+\dot{z}_2) - \frac{1}{d_2}\boldsymbol{\varepsilon}^T\boldsymbol{\varepsilon} \\ &\quad +\widetilde{\theta}_l(z_1\lambda_2-\frac{1}{g_l}\dot{\widehat{\theta}}_l)+\widetilde{\boldsymbol{\theta}}_u^T(z_1\nu_2^T-\frac{1}{g_u}\dot{\widehat{\boldsymbol{\theta}}}_u). \end{aligned} \tag{26}$$

For compactness of notation, define $c_1^* = c_1 + d_1$ and define the control term as

$$\alpha_2 = \Big(\sum_{i=1}^{L}\sigma_i(y)\boldsymbol{B}^T(u_i)\Big)\widehat{\boldsymbol{\theta}}_u. \tag{27}$$

Once α_2 is determined, u_i is computed using (27), just as in (6), for $1 \le i \le L$.

Using α_2, the $(z_1 + \dot{z}_2)$ term can be expanded as

$$(z_1+\dot{z}_2) = z_1 + \frac{d}{dt}\Big(\nu_2\widehat{\boldsymbol{\theta}}_u\Big) - \dot{\alpha}_1 - \ddot{y}_r$$

$$
\begin{aligned}
&= z_1 + \dot{\nu}_2\widehat{\boldsymbol{\theta}}_u + \nu_2\dot{\widehat{\boldsymbol{\theta}}}_u - \frac{\partial\alpha_1}{\partial y}\dot{y} - \frac{\partial\alpha_1}{\partial y_r}\dot{y}_r - \frac{\partial\alpha_1}{\partial\xi_2}\dot{\xi}_2 - \frac{\partial\alpha_1}{\partial\lambda_2}\dot{\lambda}_2 - \frac{\partial\alpha_1}{\partial\widehat{\theta}_l}\dot{\widehat{\theta}}_l - \ddot{y}_r \\
&= z_1 + \Big(-k_2\nu_1 + \sum_{i=1}^{L}\sigma_i(y)\boldsymbol{B}^T(u_i)\Big)\widehat{\boldsymbol{\theta}}_u + \nu_2\dot{\widehat{\boldsymbol{\theta}}}_u + c_1^*\Big(\xi_2 + \lambda_2\theta_l + \nu_2\boldsymbol{\theta}_u + \varepsilon\Big) \\
&\quad - c_1^*\dot{y}_r + (-k_2\xi_1 + k_2 y) + \widehat{\theta}_l\Big(-k_2\lambda_1 + \sigma_l(y)\Big) + \lambda_2\dot{\widehat{\theta}}_l - \ddot{y}_r \\
&= \alpha_2 + z_1 - k_2(\xi_1 + \lambda_1\widehat{\theta}_l + \nu_1\widehat{\boldsymbol{\theta}}_u) + c_1^*(\xi_2 + \lambda_2\widehat{\theta}_l + \nu_2\widehat{\boldsymbol{\theta}}_u) + c_1^*(\lambda_2\widetilde{\theta}_l + \nu_2\widetilde{\boldsymbol{\theta}}_u) \\
&\quad - c_1^*\dot{y}_r + k_2 y + \sigma_l\widehat{\theta}_l - \ddot{y}_r + c_1^*\varepsilon_2 + \lambda_2\dot{\widehat{\theta}}_l + \nu_2\dot{\widehat{\boldsymbol{\theta}}}_u. \qquad (28)
\end{aligned}
$$

and the control α_2 is defined to cancel most of the terms in (28),

$$
\begin{aligned}
\alpha_2 &= -c_2z_2 - d_2(c_1^*)^2z_2 - \Big(z_1 - k_2(\xi_1 + \lambda_1\widehat{\theta}_l + \nu_1\widehat{\boldsymbol{\theta}}_u) + c_1^*(\xi_2 + \lambda_2\widehat{\theta}_l + \nu_2\widehat{\boldsymbol{\theta}}_u) \\
&\quad - c_1^*\dot{y}_r + k_2 y + \sigma_l\widehat{\theta}_l - \ddot{y}_r + \lambda_2 g_l\tau_l + \nu_2 g_u\boldsymbol{\tau}_u\Big), \qquad (29)
\end{aligned}
$$

where τ_l and $\boldsymbol{\tau}_u$ are defined below. Substituting (29) into (28) leaves

$$
\begin{aligned}
(z_1 + \dot{z}_2) &= -c_2z_2 - d_2c_1^*z_2 + c_1^*\Big(\lambda_2\widetilde{\theta}_l + c_1^*\varepsilon_2 + \nu_2\widetilde{\boldsymbol{\theta}}_u\Big) \\
&\quad - \Big(\lambda_2 g_l\tau_l + \nu_2 g_u\boldsymbol{\tau}_u\Big) + \lambda_2\dot{\widehat{\theta}}_l + \nu_2\dot{\widehat{\boldsymbol{\theta}}}_u, \qquad (30)
\end{aligned}
$$

which in turn is substituted into $\dot{V}_2$ to give

$$
\begin{aligned}
\dot{V}_2 &\leq -c_1z_1^2 - c_2z_2^2 - \frac{3}{4d_1}\boldsymbol{\varepsilon}^T\boldsymbol{\varepsilon} - d_2(c_1^*)^2z_2^2 + z_2c_1^*\varepsilon_2 - \frac{1}{d_2}\boldsymbol{\varepsilon}^T\boldsymbol{\varepsilon} + z_2c_1^*(\lambda_2\widetilde{\theta}_l + \nu_2\widetilde{\boldsymbol{\theta}}_u) \\
&\quad + z_2\Big(-(\lambda_2 g_l\tau_l + \nu_2 g_u\boldsymbol{\tau}_u) + \lambda_2\dot{\widehat{\theta}}_l + \nu_2\dot{\widehat{\boldsymbol{\theta}}}_u\Big) + \widetilde{\theta}_l(z_1\lambda_2 - \dot{\widehat{\theta}}_l) + \widetilde{\boldsymbol{\theta}}_u^T(z_1\nu_2^T - \dot{\widehat{\boldsymbol{\theta}}}_u) \\
&= -c_1z_1^2 - c_2z_2^2 - \frac{3}{4d_1}\boldsymbol{\varepsilon}^T\boldsymbol{\varepsilon} - d_2(z_2c_1^* - \frac{1}{2d_2}\varepsilon_2)^2 + \frac{1}{4d_2}\varepsilon_2 - \frac{1}{d_2}\boldsymbol{\varepsilon}^T\boldsymbol{\varepsilon} \\
&\quad - \lambda_2z_2g_l(\tau_l - \frac{1}{g_l}\dot{\widehat{\theta}}_l) + \widetilde{\theta}_l(c_1^*z_2\lambda_2 + z_1\lambda_2 - \frac{1}{g_l}\dot{\widehat{\theta}}_l) \\
&\quad - \nu_2z_2g_u(\boldsymbol{\tau}_u - \frac{1}{g_u}\dot{\widehat{\boldsymbol{\theta}}}_u) + \widetilde{\boldsymbol{\theta}}_u^T(c_1^*z_2\nu_2^T + z_1\nu_2^T - \frac{1}{g_u}\dot{\widehat{\boldsymbol{\theta}}}_u) \\
&\leq -c_1z_1^2 - c_2z_2^2 - \frac{3}{4d_1}\boldsymbol{\varepsilon}^T\boldsymbol{\varepsilon} - \frac{3}{4d_2}\boldsymbol{\varepsilon}^T\boldsymbol{\varepsilon} \\
&\quad - \lambda_2z_2g_l(\tau_l - \frac{1}{g_l}\dot{\widehat{\theta}}_l) + \widetilde{\theta}_l(c_1^*z_2\lambda_2 + z_1\lambda_2 - \frac{1}{g_l}\dot{\widehat{\theta}}_l) \\
&\quad - \nu_2z_2g_u(\boldsymbol{\tau}_u - \frac{1}{g_u}\dot{\widehat{\boldsymbol{\theta}}}_u) + \widetilde{\boldsymbol{\theta}}_u^T(c_1^*z_2\nu_2^T + z_1\nu_2^T - \frac{1}{g_u}\dot{\widehat{\boldsymbol{\theta}}}_u). \qquad (31)
\end{aligned}
$$

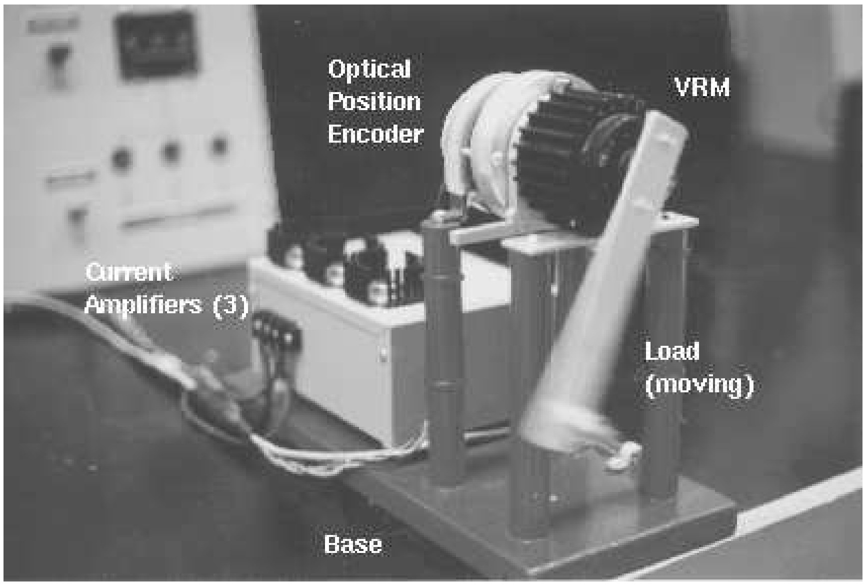

Figure 1: VRM testbed.

Defining the tuning functions $\tau_l = (c_1^* z_2 + z_1)\lambda_2$ and $\boldsymbol{\tau}_u = (c_1^* z_2 + z_1)\nu_2^T$, we have

$$\begin{aligned} \dot{V}_2 &\leq -c_1 z_1^2 - c_2 z_2^2 - (\frac{3}{4d_1} + \frac{3}{4d_2})\boldsymbol{\varepsilon}^T\boldsymbol{\varepsilon} \\ &\quad + (\widetilde{\theta}_l - \lambda_2 z_2 g_l)(\tau_l - \frac{1}{g_l}\dot{\widehat{\theta}}_l) + (\widetilde{\boldsymbol{\theta}}_u^T - \nu_2 z_2 g_u)(\boldsymbol{\tau}_u - \frac{1}{g_u}\dot{\widehat{\boldsymbol{\theta}}}_u). \end{aligned} \tag{32}$$

Thus, we have defined the control and update laws

$$\begin{aligned} \Big(\sum_{i=1}^{L}\sigma_i(y)\boldsymbol{B}^T(u_i)\Big)\widehat{\boldsymbol{\theta}}_u &= -c_2 z_2 - d_2(c_1^*)^2 z_2 - \Big(z_1 - \ddot{y}_r - k_2(\xi_1 + \lambda_1\widehat{\theta}_l + \nu_1\widehat{\boldsymbol{\theta}}_u) + k_2 y \\ &\quad + c_1^*(\xi_2 + \lambda_2\widehat{\theta}_l + \nu_2\widehat{\boldsymbol{\theta}}_u) - c_1^*\dot{y}_r + \sigma_l\widehat{\theta}_l + \lambda_2 g_l\tau_l + \nu_2 g_u\boldsymbol{\tau}_u\Big) \end{aligned} \tag{33}$$

$$\dot{\widehat{\theta}}_l = g_l\tau_l = (c_1^* z_2 + z_1)\lambda_2 \tag{34}$$

$$\dot{\widehat{\boldsymbol{\theta}}}_u = g_u\boldsymbol{\tau}_u = (c_1^* z_2 + z_1)\nu_2^T, \tag{35}$$

and have shown that

$$\dot{V}_2 \leq -c_1 z_1^2 - c_2 z_2^2 - (\frac{3}{4d_1} + \frac{3}{4d_2})\boldsymbol{\varepsilon}^T\boldsymbol{\varepsilon}. \tag{36}$$

2 Experimental Results

Illustrated in Figure 1, the VRM testbed has $P = 8$ poles and $L = 3$ phases. It is a small, bench-top motor with a maximum phase current of approximately 2A, and maximum torque of approximately 0.5 Nm. A pendulum attached to the rotor provides a gravitational load. Each phase is driven by a linear analog current amplifier, constructed from a power operational amplifier (LM30CLK). Each amplifier is driven in turn by a D/A converter (MultiQ, Quanser), which is housed in a 486-class PC running DOS. The rotor's angular position is measured with an optical encoder (E25BB-6R-2540, BEI Motion Systems), whose output is decoded by the MultiQ board. The adaptive controllers are realized in C code, which runs on a TMS320C30 DSP board (Spectrum), which is also housed in the PC. (The PC's microprocessor is not used to implement the controllers.) The sampling frequency is fixed at 400Hz. For both experiments, the desired position is $y_r(t) = \pi - \pi\cos(\pi\, t/2)$, which rotates the load smoothly between 0 and 2π rad.

Pertinent parameters of the full-state experiment are listed in Table 1. Note that the linear gains $c_{f1} = 25$ and $c_{f2} = 10$ place the "outer-loop" poles at -5, which is a relatively low gain for this plant. These gains can be increased so that both poles are at -25, for example, resulting in a much smaller transient and steady-state tracking error. However, this would mask the performance of the adaptive part of the system, which we seek to illustrate. For both experiments, the gravity parameter $\widehat{\theta}_l$ is initialized at approximately 15% of its "true" value, and the winding parameters are initialized approximately 200% of what would be a reasonably good model of the torque-position-current relation. Thus, there is significant initial parameter error. The velocity filter (10) has $\omega_0 = 150$, which is significantly larger than the bandwidth of the desired trajectory.

Experimental results are plotted in Figures 2-4. After an initial transient, the tracking error converges to a steady-state periodic signal with amplitude less than 0.2 rad. This error is due to several factors, including unmodeled dynamics (the relation among torque, rotor position and winding current has higher-order Fourier harmonics [9]), and, more importantly, the dynamics of (10). This latter observation can be confirmed by simulating a model of the system, and comparing the steady-state error with that obtained when the actual velocity is

Table 1: Design Parameters for the Full-State Experiment.

Description	**Value**
Number of B-spline basis functions	$M = 5$
Interval size for B-splines	$\delta = 0.25\text{A}$
Outer-loop gains	$c_{f1} = 25\,,\ c_{f2} = 10$
Velocity filter cut-off	$\omega_0 = 150$ rad/s
Liapunov Q matrix	$Q = \begin{bmatrix} 15 & 0 \\ 0 & 1 \end{bmatrix}$
Initial state	$\boldsymbol{x}_0 = [0\ \ 0]^T$
Initial load estimate	$\hat{\theta}_l = 10$
Initial winding parameters	$\hat{\theta}_{uj} = 50 \cdot j$
Adaptation gains	$g_u = 50\,,\ g_l = 50$

used in feedback. When this is done, the maximum (L_∞) steady-state tracking error for the controller that uses the actual rotor velocity is about 50% of that obtained when using the filtered velocity estimate. Thus, for adaptive VRM control, the "dirty derivative" method of "measuring" velocity using (10) strongly affects performance.

In practice, we find that increasing ω_0 causes unmodeled dynamics in the motor to be excited, resulting in an audible high-frequency vibration as the rotor turns. This is probably the stator poles vibrating. Decreasing ω_0 reduces this noise, but results in an increased steady-state tracking error. We remark that a dead-zone could be introduced to prevent the slight parameter drift that results.

Parameters for the observer-based controller are listed in Table 2. The initial parameter estimates and initial states are identical to the full-state experiment. The gains c_1 and c_2 are chosen so that the eigenvalues are at -5, just as for the full-state case. The "observer poles" are placed at -15, and the damping gains d_1 and d_2 are relatively small, to ensure a fair comparison. Finally, the adaptation gains are set so that the parameters evolve at a rate similar to that in the full-state experiments. However, since each controller has a different tuning function, it is difficult to define adaption gains that are the same for both experiments.

Table 2: Design Parameters for the Observer-Based Controller.

Description	**Value**
Liapunov gains	$c_1 = 6\,,\ c_2 = 4$
Observer gains	$k_1 = 30\,,\ k_2 = 225$
Damping gains	$d_1 = 1\,,\ d_2 = 1$
Adaptation gains	$g_l = 20\,,\ g_u = 20$

Experimental results are plotted in Figures 5-7, using the same scale as in Figures 2-4. A comparison shows that the observer-based controller provides a superior transient response, despite the additional observer dynamics. Moreover, the steady-state tracking error z_1 is approximately half that seen in the full-state experiment. We remark that, although the observer states are initialized at the "true" initial condition (the origin), the observer error dynamics are excited, i.e., $\boldsymbol{\varepsilon}$ moves away from the origin, because $\ddot{y}_r$ is discontinuous at $t = 0$.

One final advantage of the observer-based control is not apparent from the plots: During the observer-based control experiment, the motor is quieter in an audible sense than during the full-state experiment. Apparently, the full-state controller causes the stator poles to vibrate because of its wide bandwidth. On the other hand, the observer-based controller "rolls-off" the closed-loop dynamics, preventing excitation of high-frequency unmodeled dynamics.

3 Conclusions

A review of the literature indicates that backstepping is applied largely to electro-mechanical systems, e.g. motors. In practice, states of these systems include positions and velocities; often only the former is directly measured. It is common practice to differentiate this signal to produce an estimate of velocity, and then apply results that require full-state measurement. This paper illustrates the pitfalls such an approach with the VRM, and the advantages of using the recently developed output-measurement adaptive backstepping methods.

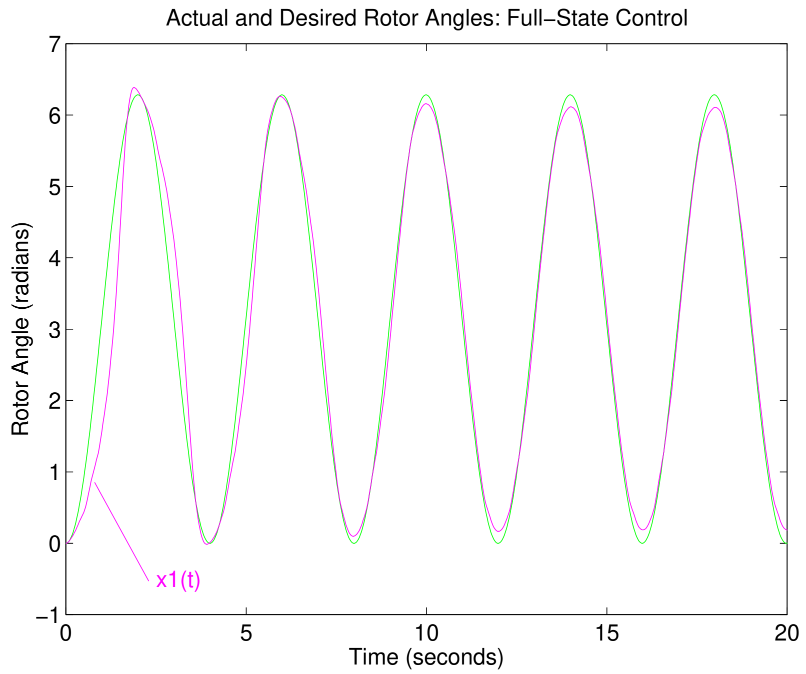

Figure 2: Desired rotor position $y_r(t)$ and actual rotor position $y(t)$ for the full-state controller described in Section 1.1.

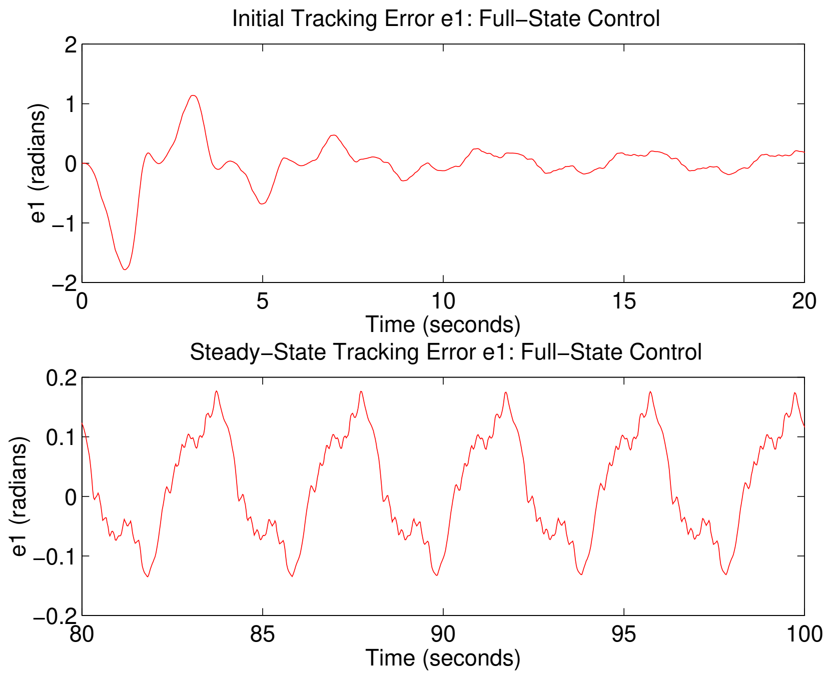

Figure 3: Initial and "steady-state" tracking error e_1 for the full-state controller.

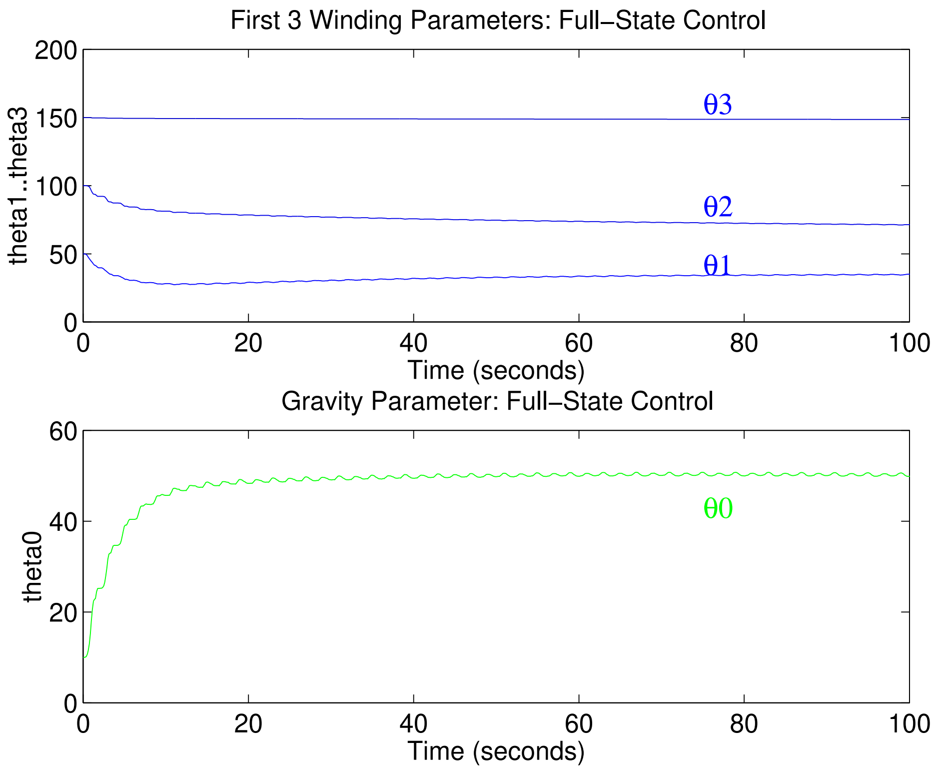

Figure 4: Winding and gravity parameter estimates for the full-state controller described in Section 1.1. The gravity parameter $\widehat{\theta}_l$ is initialized at 10, while its "true value" is approximately 70. The winding parameters are initialized at roughly twice values that would be considered close to "true."

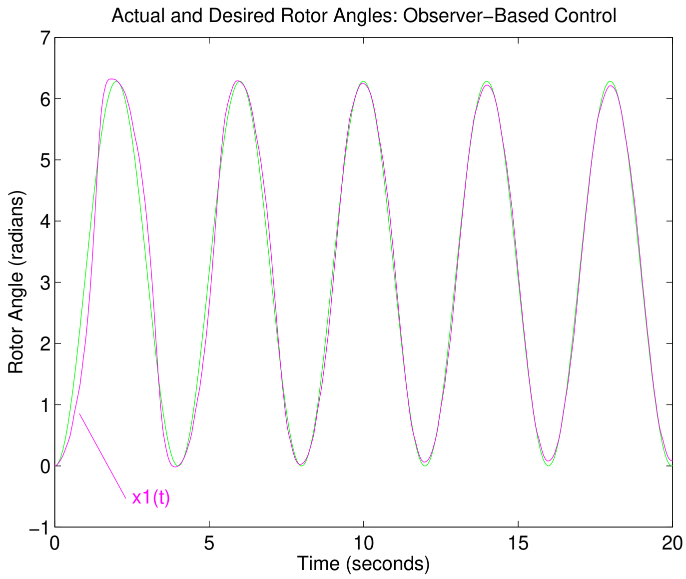

Figure 5: Desired rotor position $y_r(t)$ and actual rotor position $y(t)$ for the observer-based controller described in Section 1.2.

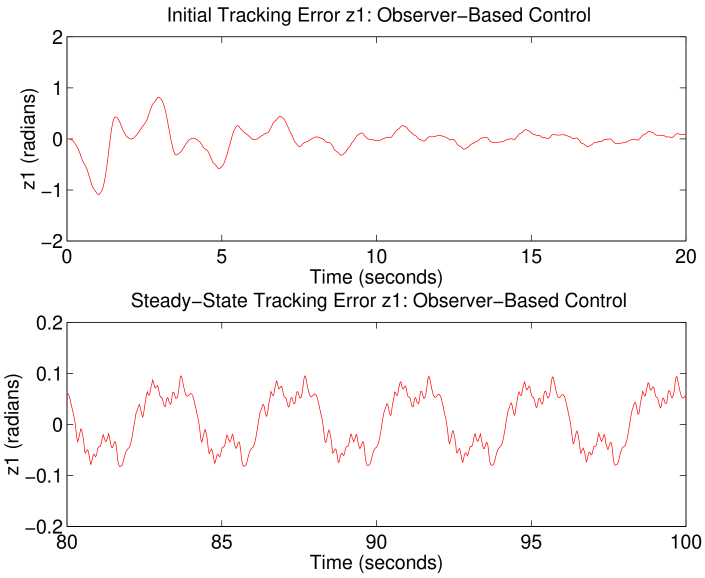

Figure 6: Initial and "steady-state" tracking error z_1 for the observer-based controller.

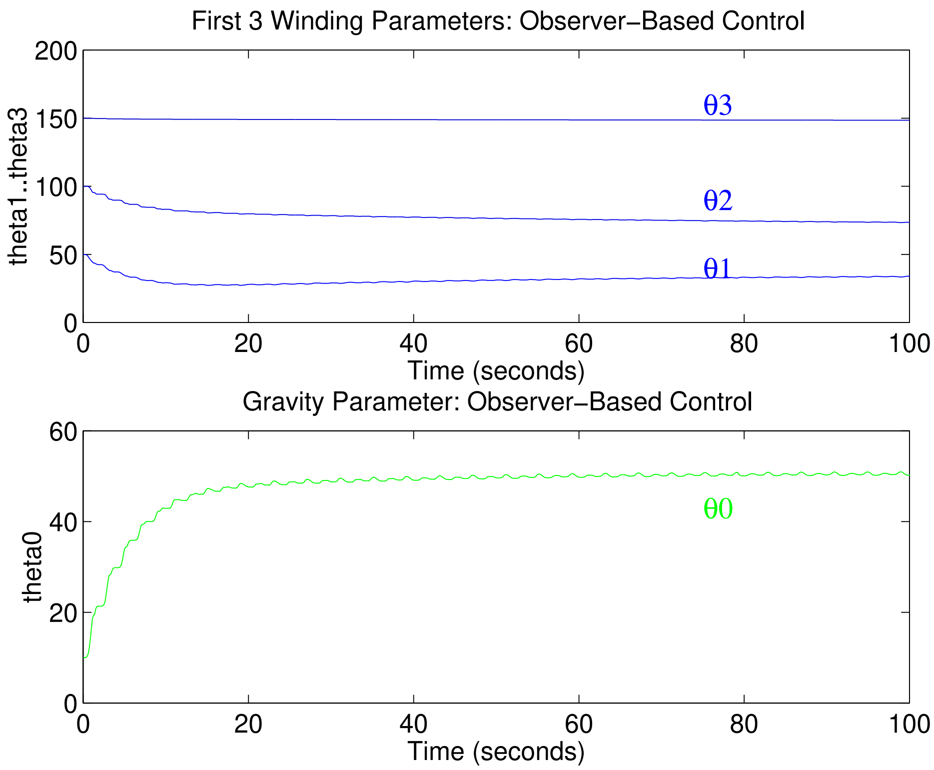

Figure 7: Winding and gravity parameter estimates for the observer-based controller described in Section 1.2. The gravity parameter $\widehat{\theta}_l$ is initialized at 10, while its "true value" is approximately 70. The winding parameters are initialized at roughly twice values that would be considered close to "true."

References

[1] M. Krstić, I. Kanellakopoulos, and P. Kokotović, *Nonlinear and Adaptive Control Design*. Wiley, 1995.

[2] R. Marino, S. Peresada, and P. Tomei, "Output feedback control of current-fed induction motors with unkown rotor resistance," *IEEE Transactions on Control Systems Technology*, vol. 4, pp. 348–362, July 1996.

[3] M. Ilic-Spong, R. Marino, S. M. Peresada, and D. Taylor, "Feedback linearizing control of switched reluctance motors," *IEEE Transactions on Automatic Control*, vol. AC-32, pp. 371–379, May 1987.

[4] M. Leviner, D. Dawson, and J. Hu, "Position tracking control of a switched reluctance motor using partial state feedback," in *Proceedings of the 1994 American Control Conference*, vol. 3, (Baltimore, MD), pp. 3095–9, July 1994.

[5] J. Carroll, D. Dawson, and P. Vedaqarbha, “Experimental verification of adaptive and robust trajectory tracking controllers for switched reluctance motors,” in *Proceedings of the 33rd IEEE Conference on Decision and Control*, vol. 2, (Lake Buena Vista, FL), pp. 1856–61, Dec. 1994.

[6] R. R. Kohan and S. A. Bortoff, “Adaptive control of variable reluctance motors using spline functions,” in *Proceedings of the 1994 Conference on Decision and Control*, (Lake Buena Vista, Florida), pp. 1694–1699, Dec. 1994.

[7] M. Bridges and D. Dawson, “Adaptive control of rigid-link electrically driven robots actuated with switched reluctance motors,” in *Proceedings of the 1995 American Control Conference*, vol. 2, (Evanston, IL), pp. 1392–6, June 1995.

[8] J. Carroll, A. Geogham, D. Dawson, and P. Vedagarbha, “A backstepping based computed torque controller for switched reluctance motors driving inertial loads,” in *Proceedings of the 4th IEEE Conference on Control Applications*, (Albany, NY), pp. 779–786, Sept 1995.

[9] S. A. Bortoff, R. R. Kohan, and R. Milman, “Adaptive control of variable reluctance motors: A spline function approach,” submitted to *IEEE Transactions on Industrial Electronics*, 1996. Preliminary version available on the WWW at `http://www.control.toronto.edu/ bortoff`.

[10] J. Lin and I. Kanellakopoulos, “Adaptive nonlinear control in active suspensions,” in *Proceedings of the 1996 IFAC*, (San Francisco, USA), pp. 113–118, July 1996.

[11] R. Bupp, D. Bernstein, and V. Coppola, “Experimantal implementation of integrator backstepping and passive nonlinear controllers on the rtac testbed,” in *Proceedings of the 1996 IEEE Conference on Control Applications*, pp. 279–284, 1996.

[12] M. Krstić and P. Kokotović, “Adaptive nonlinear output-feedback schemes with marino-tomei controller,” *IEEE Transactions on Automatic Control*, vol. 41, pp. 274–80, Feb. 1996.

[13] D. G. Taylor, “An experimental study on composite control of switched reluctance motors,” *IEEE Control Systems Magazine*, vol. 11, pp. 31–36, Feb. 1991.